Journal of Heat and Mass Transfer Research

Journal homepage: http://jhmtr.semnan.ac.ir

Semnan University

The Effect of SiO_2 Nanoparticle on the Performance of Photovoltaic Thermal System: Experimental and Theoretical Approach

Ali Esmaeilinasab[a], Aminreza Noghrehabadi [a], Mojtaba Moravej[*,b], Ebrahim Khajehpour[c]

[a] *Department of mechanical engineering, shahid chamran University of Ahvaz, Ahvaz, Iran.*
[b] *Department of mechanical engineering, Payame noor University, Iran.*
[c]*Department of Mechanical Engineering, Islamic Azad University, Tehran South Branch, Tehran, Iran.*

PAPER INFO

Paper history:
Received: 2019-10-11
Revised: 2020-01-26
Accepted: 2020-02-01

Keywords:
Domestic photovoltaic-thermal system;
Nanofluid;
Thermal and electrical efficiency;
Experimental;
Theoretical.

ABSTRACT

The low conversion efficiency of solar cells produces large amounts of thermal energy to the cells, and with an increase in the temperature of solar cells, their electrical efficiency decreases. Therefore, a hybrid photovoltaic thermal (PVT) system ameliorates the total performance of the system by adding thermo equipment to the solar cell and removing excessive heat from these cells. In this paper, we inspect SiO_2/water nanofluids effect on the electrical and thermal efficiency of domestic photovoltaic thermal systems (DPVT) theoretically and experimentally. In the theoretical part, as a result of the control-volume finite-difference (CVFD) method, an explicit dynamic model was extended for a flat-plate collector, which is added to the photovoltaic panel with a closed-loop cooling system with withdrawing urban water from the storage tank. The model accuracy was verified in comparison with the measured experimental data. Experimental results indicate that by increasing the concentrations of nanofluid, the thermal and electrical performance has improved, and overall efficiency decreased by increasing the diameter of the nanoparticles. The overall efficiency of the DPVT for 0 and 3 weight percent of SiO_2/ water nanofluids with a diameter of 11-14 nanometers enhanced to 5.4% and 7.76% compared to the base fluid, respectively.

DOI: 10.22075/jhmtr.2020.18904.1254

1. Introduction

One of the basic problems of solar cells is reducing electrical efficiency due to an increase in temperature. Solar cells usually have low energy conversion efficiency, with a low rate of heat production. Therefore, this extra energy will increase the temperature of the cells. The electrical efficiency of these cells can be increased by cooling the heat removed from the cells that can be applied to produce domestic hot water or space heating. Employing the dual system of producing electricity and heat is not new and dates back to the early recognition of solar cells and solar thermal systems. Research on heat removal and an increase in the efficiency of photovoltaic cells began before 1970. In the very recent decade, A number of studies have been demonstrated on hybrid and hybrid systems in order to boost both economic and thermal efficiency. A photovoltaic- thermal system can be constructed by combining solar cells and thermal components. In fact, photovoltaic cells play a role in heat absorber in this type of system. The purpose of this combination is to apply the heat present in the cell for other applications. In addition, the hybrid design can stabilize current and voltage and reduce thermal stresses to increase efficiency. So far, many theoretical [1-9] studies have been conducted to evaluate the performance of photovoltaic systems. Water in most experimental and theoretical research has been employed in order to amend the performance of solar cells.

Borane et al. [1] did some research on the design of a photovoltaic/thermal and economical collector that worked with air. They have proven to be better in terms of

[*]*Corresponding Author: Mojtaba Moravej, Department of mechanical engineering, Payame noor University, Iran.*
Email: moravej60@pnu.ac.ir

energy and cost for the eight regions in Europe than traditional models. The simulation also yielded some interesting results regarding the reduction of primary energy consumption, the reduction of carbon dioxide production, and the return on investment.

Chen et al. [2], in his study, explored the solar trigeneration models in order to PVT for Pseudo-warm climates. They showed that the model set up as a result of glazed photovoltaic solar collectors interconnected by a chiller with a half-effect absorption layout give the 0.072 for COP and the highest solar utilization factor of 0.241. Dupeyrat et al. [3] had a theoretical inspection of the electrical and thermal performances of some flat plate PVT with a single glaze. They utilize water as a coolant and applying a 2D simple model. In their work, several ways presented to improve efficiency, which consists of the different methods of heat transfer between coolant and PV cells, and on the optical properties of materials as well. Boubekri et al. [4] developed a mathematical model based on the principle of heat transfer in which the thermal behavior of photovoltaic- thermal system components examined. In their research, the effect of the mass flow rate of coolant, heat transfer coefficient of layer, and value of the inclination angle on the overall efficiency of the collector were inspected. In the new study, Bhattarai et al. [5] developed a simulation method of the transient heat transfer of the tube and sheet in a PVT set by a 1-D mathematical model.

In this study, the operation and performance of PVT and conventional solar collecting systems are inquired theoretically and experimentally. All models of the PVT system were proposed for fluid flow in an open-loop without removing the water from the storage tank.

Bokor et al. [10] analyzed the passive cooling effect of transpired solar collectors, theoretically and experimentally. They conclude that the passive cooling effect of the transpired solar collector is increasing with rising intensity of radiation, as the heat transfer coefficient between the plenum and the backplate decreases with increasing solar radiation.

Subsequently, Chow et al. [11] conducted experimental research of PVT. They examined the water-heating system with different operating modes at different times. They concluded that water with natural circulation was more efficient than the forced circulation type in this hybrid system. They did their experiments in Hong Kong late summer and also found that the thermal performance was 38.9% at zero decreased temperature, and the corresponding electricity performance was 8.56%.

Rezvanpour et al. [12] used phase changed materials to increase the performance of photovoltaic panels. The PCMs decreased the temperature of panels by about 38%, and the outlet power enhanced about 24%. They also used TRANSYS software to modeling and validated their work and proved the highlighted error was less than 9%.

He and colleagues [13] indicated in an experimental study that the daily thermal performance of sheets and tubes for a PVT system under normal water circulation has been discovered to be about 40%, of which about 75% is for a conventional solar thermosiphon solar collector system. The average daily electrical performance is found to be about 10%, which is lower than that of the traditional monocrystalline silicon photovoltaic plate under the same conditions. Abbas et al. [14] studied using nanofluid in photovoltaic thermal collector on a large scale. They showed that at higher velocity laminar flows of coolant, the maximum efficiency could be obtained.

Noghrehabadi et al. [15] investigated the influence of the urban water rate on the electrical and thermal efficiency of the domestic photovoltaic thermal (DPVT) system with water as the coolant. Experimental results demonstrate an increase in the amount of urban water consumption reduces the average temperature of the PVT system to the temperatures close to the temperature of ambient. Furthermore, the electrical output increases by reducing the average temperature of the PVT system and, as a result reducing the temperature of the cell. We found out that by increasing the consumption of urban water, thermoelectrical efficiency increased by 2% and 0.4%, respectively.

Since one of the major parameters in the PVT system is the type of working fluid, in recent years, nanofluid has been applied to ameliorate the performance of these systems. Karimi and Rahimi [16] demonstrated an examination in order to evaluate the cooling efficiency of Boehmite ($AlOOH•xH_2O$) nanofluid –water based in a hybrid PV cell. They compared cooling performances of water as the base fluid and three different concentrations in range 0.01, 0.1, and 0.3 wt%.

They evaluated the thermal performance of nanofluids based on the results acquired from the output current temperature and the mean surface temperature of the PV. Their results showed that the mean surface temperature of PV decreased from 62.29 ° C to 32.5 ° C at zero and 300 ml/min, respectively, for the 0.01 wt% nanofluid flow rate. In addition, the greatest improvement in electrical efficiency was achieved at about 27% for a concentration of 0.01 wt% of nanofluids at this flow rate.

Sardarabadi et al. [17] inquired about the effects of applying nanofluids as a coolant on the thermo electrical efficiency of a photovoltaic thermal unit. The coolants in their experiments are pure water and silica (SiO_2) / nanofluid water of 1% and 3% by weight (% w). They indicated that the overall energy efficiency increase for silica/water nanofluids was 1 wt% and 3 wt% 3.6% and 7.9%, respectively, compared to pure water.

The thermal efficiency of the PVT collector increased up to 7.6% and 12.8%, for two cases of 1 wt% and 3 wt% of SiO_2/water nanofluids, respectively. Moreover, they computed that by adding a water heater collector to a PV system, the total exergy increased up to 19.36%, 22.61%, and 24.31% for the three cases of pure water, 1 wt% SiO_2/water nanofluid, and 3 wt% silica/water nanofluid, respectively. Numerical simulation of the cooling of a solar cell by forced convection in the presence of an Al_2O_3/water Nanofluid was inspected by Elmir et al. [6].

In their work, equations governing heat transfer and flow hydrodynamics are as interpreted by the energy and Navier-Stockes equations. They inquired the solid volume fraction effect for different values of Reynolds number on the results in the form of isotherms and modified local and average Nusselt number. The suspension of nanoparticle and base fluid caused to enhance in the value of heat transfer thus the meliorating cooling of the solar cells leads to having a good performance of the solar panel. Xu and Kleinstreuer [18] inspected computationally the thermal efficiency of the densely packed photovoltaic cells under high concentration by applying the Al_2O_3-water cooling system. They evaluated the effect of operational parameters and different system designs. Their study consisted of a semi-empirical nanofluid model for the thermal conductivity and pump power and performance to improve efficiency. The modest system efficiency in their research was 20%. Moreover, their results indicated lower nanofluid inlet temperatures and higher nanoparticle volume fractions further improve the cell efficiency and suggested a combined concentration photovoltaic and thermal heating system for complete solar energy use.

In the present study, a Domestic Photovoltaic-thermal (DPVT) collector with a closed-loop cooling system designed and built. Water/ SiO_2 nanofluid is applied as a working fluid in a closed-loop cooling system. SiO_2 nanoparticles are used because of cheapness and excellent sustainability in water. Furthermore, for the first time as the result of the CVFD method, an explicit dynamic prototype is developed for a flat-plate collector PVT system with water/ SiO_2 nanofluid as the coolant and withdrawing water from the storage tank. In the experimental part of this paper, by alternating the concentration of nanofluids, the average diameter of the nanoparticles in nanofluids and urban water consumption rate, the thermoelectrical performance of photovoltaic-thermal systems are explored. This work can be counted as a compact investigation on the thermoelectrical performance of the PVT system as there are not many reports in this field in literature, and all of them have reported some of the affecting parameters. To make it simple, the affecting parameters such as nanoparticles diameter, mass concentration, the consumption rate of urban water have not been inquired simultaneously in literature.

2. Photovoltaic-thermal system and measurement rig

DPVT system is composed of two electrical and thermal parts. In this work, a water-type hybrid collector was constructed and examined with a polycrystalline PV module on a sheet-tube type thermal absorber. The electrical part is a 60W photovoltaic Panel with Poly Crystalline technology, and the thermal part is similar to a conventional solar collector. The image of PVT collector presented in Fig. 1. The thermal part consists of a sheet and tube heat exchanger under the solar cell and a circular

Figure 1. A View of the Experimental equipment.

heat exchanger in the storage tank. Working fluid in a closed-loop path is applied for cooling the photovoltaic panel. The storage tank of hot water is directly connected to the urban water, which passes over the heat exchanger in the tank. The heat exchanger is placed under the solar cell, and it consists of a copper sheet and twelve copper pipes. A layer of insulation is placed behind the system. The heat exchanger is insulated as well, and a glass plate is located above the photovoltaic panel.

To measure thermal efficiency, two thermocouples (K type) were located at the outlet and inlet of the heat exchanger. Temperatures of the thermal components of DPVT system such as photovoltaic panel, the copper plate, the copper pipe, and the fluid inside the heat exchanger are measured by thermocouples which were placed in the middle of them. Thermocouples were connected to a 4-channel data logger (176T4-Testo model). An aquarium pump was used for fluid circulating (DWI) inside the closed-loop cooling system. The TES 132 solar meter type was employed in order to track the solar radiation. Solar panel output voltage and current were measured and recorded by two multi-meters. A controller was applied so voltage and current can be controlled. Finally, all the measurement data were transferred to a PC. Fig. 2 depicted the schematic diagram and set up of DPVT system experiment rig.

In this study, to ameliorated the performance of the photovoltaic-thermal system, nanofluids including SiO_2 nanoparticles (11-14 nm and 60-70 nm) have been applied. Characterizations of nanoparticles used for preparation of

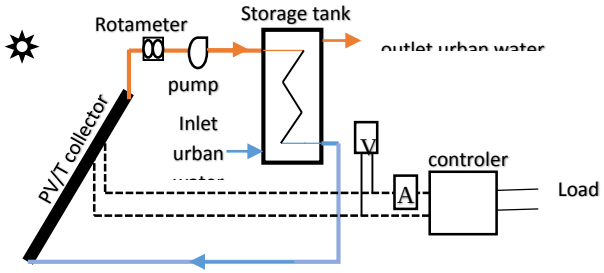

Figure 2. Schematic diagram of photovoltaic thermal system experiment rig.

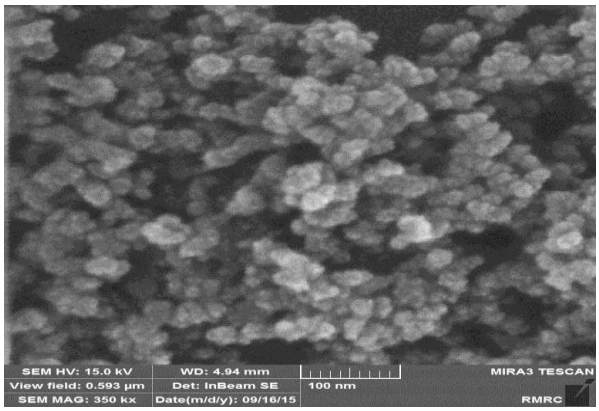

(a)

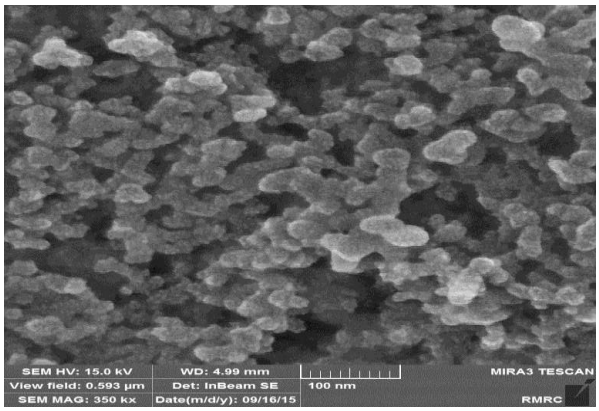

(b)

Figure 3. The SEM micrograph of SiO_2 nanoparticles a. 11-14 nm b. 60-70 nm

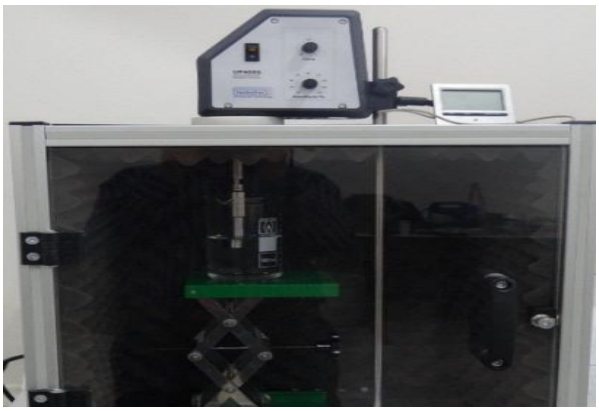

(a)

(b)

Figure 4. Apparatus for the preparation of nanofluids a. ultrasonic b. homogenizer.

nanofluids are displayed in the table 1. Moreover, SEM micrograph of both SiO_2 nanoparticles are illustrated in Fig. 3.

Apparatuses for the preparation of nanofluids are homogenizer (Micra), and ultrasonic (Ohaus). These devices are depicted in Fig. 4.

3. Mathematical modeling of the photovoltaic-thermal system

An explicit dynamic prototype method was developed as a result of the CVFD method for a single-glazed flat-plate PV/T collector with a closed-loop cooling system. The entire photovoltaic-thermal system was discretized into eight components types 1. glass cover 2. photovoltaic panel 3. cooper plate 4. cooper pipe 5. working fluid in duct 6. insolation 7. storage tank 8. Galvanized cover. Fig. 5. shows an in-depth geometrical description of PVT absorber used in this work.

In order to simplify system modeling, Subsets of each component are considered proportional to each other so that the mean value for each component is deliberated. In fact, in this modeling, the temperature of each component is an average value for the whole of that component, and the features of each component only alternate over time. All main equations for each component are adopted from the steady-state energy balance. For glass cover (g) Eq. (1) was acquired as follows:

$$\delta_g \rho_g C_{p\,g} \frac{dT_g}{dt} = G\alpha_g + h_{r,g-s}\left(T_s - T_g\right) + h_{wind}\left(T_a - T_g\right) + \left(h_{cv,pv-g} + h_{r,pv-g}\right)\left(T_{pv} - T_g\right) \quad (1)$$

Where T_g, T_p, T_a are the glazing, absorber plate, and ambient temperature, respectively. G is incident solar radiation that is received by the collector, α_g is absorptivity coefficient of glass, h_{wind} and h_{c_g} are convective heat transfer coefficients at the outer and inner glass surfaces, respectively. h_{r,c_g} and h_{r,g_a} are coefficients of radiation heat transfer at the inner and outer glass surfaces, respectively. Sky temperature, the absorption coefficient of the glass cover, and the transmission coefficient are calculated by the following equations [19].

$$T_s = 0.0552 * {T_a}^{1.5} \quad (2)$$

Table 1. Characterizations of nanoparticles

Nanoparticle Type	Diameter (nm)	Purity	SSA(m^2/g)	Bulk density	Actual density
SiO_2	11-14	+99%	190-685	>0.11(g/cm^3)	2.2(g/cm^3)
SiO_2	60-70	+98%	160-600	>0.10(g/cm^3)	2.4(g/cm^3)

$$\tau_g = e^{-\lambda\delta_g/\cos\theta_2} \quad (3)$$

Where λ is the extinction coefficient and θ_2 can be calculated as [20, 24]:

$$\theta_2 = arc\sin\left(\frac{\sin\theta_1}{n_v}\right) \quad (4)$$

$$\begin{aligned}\cos\theta_1 = {} & \cos\beta(\sin\delta\sin\phi + \cos\delta\cos\phi\cos\omega) \\ & + \cos\delta\sin\omega\sin\beta\sin\gamma \\ & + \sin\beta\cos\gamma \\ & (\sin\delta\cos\phi - \cos\delta\cos\omega\sin\phi)\end{aligned} \quad (5)$$

$$\omega = 15(t_s - 12) \quad (6)$$

$$\delta = 23.45 * \sin\left[\frac{360 * (284 + N)}{365}\right] \quad (7)$$

Where t_s is the actual time of sun, and N is the number of days.

Eq. (8) has modeled the thermal behavior of the Photovoltaic panel (PV).

$$\begin{aligned}\delta_{pv}\rho_{pv}C_{p\,pv}\frac{dT_{pv}}{dt} = {} & G(\tau\alpha)_{pv} - E \\ & + h_{cd,p-pv}(T_p - T_{pv}) \\ & + \left(h_{cv,pv-g} + h_{r,pv-g}\right) \\ & (T_g - T_{pv})\end{aligned} \quad (8)$$

Where E is electrical power output, $h_{cd,p\text{-}pv}$ is the conductive heat transfer coefficient between pv panel and cooper plate. Furthermore, $(\alpha\tau)_{pv}$ is calculated by the following equation [24].

$$(\alpha\tau)_{pv} = \frac{\tau_g\tau_r\alpha_{pv}}{1 - (1 - \alpha_{pv})r} \quad (9)$$

$$\tau_r = \frac{1 - r}{1 + r} \quad (10)$$

Where τ_r and r are the transmittance and Reflection coefficient of the photovoltaic panel, respectively.

Electrical output power is computed by the Eq. (11).

$$E = G.PF.\tau_g.\eta_o \times \left[1 - \varphi_c(T_{pv} - 25)\right] \quad (11)$$

In agreement to the previous literature, the power efficiency of a single photovoltaic cell decreases roughly linearly with cell temperature, and this is the case for above 0 ˚C. The correlation for predicting the thermal behavior of the Absorber plate (P) has been obtained as realized in Eq. (12).

$$\begin{aligned}\delta_p\rho_pC_{p\,p}\frac{dT_p}{dt} = {} & h_{cd,p-pv}(T_{pv} - T_p) \\ & + \frac{A_{pt}}{A_p}h_{cd,p-t}(T_t - T_p) \\ & + (1 - D_eL)h_{cd,p-i} \\ & (T_i - T_p)\end{aligned} \quad (12)$$

The thermal behavior of cooper tube (t) has been presented as Eq. (13).

$$\begin{aligned}\delta_t\rho_tC_{p\,t}\frac{dT_t}{dt} = {} & \frac{A_{pt}}{A_t}h_{cd,p-t}(T_p - T_t) \\ & + \frac{A_f}{A_t}h_{cv,t-f}(T_f - T_t) \\ & + \frac{A_i}{A_t}h_{cd,i-t}(T_i - T_t)\end{aligned} \quad (13)$$

Where $h_{cv,t\text{-}f}$ is the coefficient of the convective heat transfer between tube and working fluid in the middle of the collector.

Thermal correlation of Working fluid (f) has been achieved as follows:

$$\begin{aligned}M_{f1}C_{p\,f1}\frac{dT_{f1}}{dt} = {} & h_{cv,t-f}A_f(T_t - T_{f1}) \\ & + \dot{m}_{f1}C_{p\,f1}(T_{f0} - T_{f2})\end{aligned} \quad (14)$$

Where T_{f0}, T_{f1} and T_{f2} are the coolant temperature at the inlet, middle and outlet of collector, respectively.

$$T_{f1} = \frac{T_{f0} + T_{f2}}{2} \quad (15)$$

Moreover, the thermal behavior of Insolation (i) has been obtained as Eq. (16).

$$\begin{aligned}M_iC_{p\,i}\frac{dT_i}{dt} = {} & h_{cd,p-i}A_{ip}(T_p - T_i) \\ & + h_{cd,i-t}A_{it}(T_t - T_i) \\ & + h_{cd,ga-i}A(T_{ga} - T_i)\end{aligned} \quad (16)$$

Eventually, the thermal correlation of galvanized cover (ga) and storage tank (tk) have been presented in Eqs. 17 and 18.

$$\begin{aligned}M_{ga}C_{p\,ga}\frac{dT_{ga}}{dt} = {} & h_{cv,ga-a}A_{ga}(T_a - T_{ga}) \\ & + h_{cd,ga-i}A_{ga}(T_i - T_{ga})\end{aligned} \quad (17)$$

$$\begin{aligned}M_{tk}C_{p\,tk}\frac{dT_{tk}}{dt} = {} & h_{cv,tk-a}A_{tk}(T_a - T_{tk}) \\ & + \dot{m}_{f1}C_{p\,f1}(T_{f2} - T_{f0}) \\ & - \dot{m}_{tk}(T_{tk} - T_{tk,i})\end{aligned} \quad (18)$$

Where T_{tk} and $T_{tk,i}$ are the temperature of urban water consumption in the middle and inlet of the storage tank. It is noteworthy to mention that boundary conditions in the present study are the ambient temperature for air and water. The initial temperature for all of air, water, and nanofluid are the ambient temperature.

3.1. Heat transfer coefficients

The coefficient heat transfer of the wind has been computed by Eq. 19, which is presented by Wattmuff et al. [25]. The experiments performed in the wind tunnel, and they introduced a correlation between wind speed and wind heat transfer coefficient.

$$h_{wind} = 2.8 + 3\,V_{wind} \quad (19)$$

Where h_{wind} and V_{wind} are the heat transfer coefficient and wind speed, respectively. Heat transfer coefficient between the cover glass and photovoltaic panel can be expressed as:

$$h_{cv,g-pv} = \frac{Nu\ k_{air}}{b} \quad (20)$$

Where k_{air} thermal conductivity of air and b is the distance between the glass cover and photovoltaic panel. Nu is the Nusselt number of air between the glass cover and photovoltaic panel, which is calculated confirming to the Grashof number by the Eqs. 21, 22 and 23 [24].

$$Gr < 1700 + 47.8\phi \qquad Nu = 1.013 \quad (21)$$

$$Gr > 80000 \qquad Nu = 2.5 + 0.0133(90 - \phi) \quad (22)$$

$$Nu = [0.06 + 3 \times 10^{-4}(90 - \phi)]Gr^{0.33} \quad (23)$$

Where ϕ the tilt angle of collector and Gr is Grashof number $n_{cv,t-f}$ is the heat transfer coefficient between the tube and working fluid which is given by:

$$h_{cv,t-f} = \frac{Nu\ k_w}{D_t} \quad (24)$$

Where k_w is the thermal conductivity of the working fluid and D_t is the inner diameter of the tube. The Eqs. (25) and (26) are employed to compute the heat transfer coefficient between urban water and helical coil heat exchanger inside the storage tank [21].

$$c_{eff} = \frac{(1-\phi)\rho_f c_f + \phi\rho_s c_s}{\rho_{eff}} \quad (36)$$

$$Nu_{o,HE.tk} = 0.989\mathrm{Re}_D{}^{0.33}\mathrm{Pr}^{0.33} \quad (25)$$

$$h_{o,HE,tk} = \frac{Nu_{o,HE,tk}K_w}{D_o} \quad (26)$$

The coefficient of the heat transfer for heat exchanger (between the working fluid and copper tube) by the Eqs. (27) to (30) is acquired.

Where *He* is modified dean number, p is the helical pitch of the coil, D_{Hc} is the diameter of the coil, and D_t is the inner diameter of the tube. The radiation heat transfer coefficient between the glass cover and photovoltaic panel by Eq. (38) is calculated.

$$h_{HC} = \left[\frac{48}{11} + \frac{{}^{51}/_{11}}{\left[1 + {}^{1342}/_{(\mathrm{Pr}.He^2)}\right]^2} + 1.816\left(\frac{He}{1 + {}^{1.15}/_{\mathrm{Pr}}}\right)^{3/2}\right]^{1/3} \quad (27)$$

$$He = Dean\,.\left[1 + \left(\frac{p}{\pi \mathrm{D}_c}\right)^2\right]^{-1/2} \quad (28)$$

$$Dean = \mathrm{Re}_D.\sqrt{{}^{D_t}/_{D_c}} \quad (29)$$

$$D_c = D_{Hc}\,.\left(1 + \left({}^{P}/_{\pi.\,D_{Hc}}\right)\right) \quad (30)$$

$$h_{r,g-pv} = \frac{\sigma\left(\theta_g^2 + \theta_{pv}^2\right)\left(\theta_g + \theta_{pv}\right)}{\frac{1}{\varepsilon_{pv}} + \frac{1}{\varepsilon_g} - 1} \quad (31)$$

Where ε_{pv} is emissivity of the photovoltaic panel. θ_g and θ_{pv} are temperature of glass cover and photovoltaic panel in Kelvin, respectively.

3.2. Characteristics of SiO_2/DI water nanofluid

In order to determine the convective heat transfer coefficient of nanofluids flowing through the duct pipe under the laminar regime, Maiga et al.'s equation [22, 23] has been employed. This correlation was developed for constant wall heat flux, laminar flow regime (Re<1000), prandtle number between 6 and 753 and volume concentration between zero and 10 percent($0 < \varphi < 10\%$). In this work, Reynolds number is about 270 and the prandtle number of nanofluids are over 7.

$$Nu_{nf} = 0.086\mathrm{Re}^{0.55}\ \mathrm{Pr}^{0.5} \quad (32)$$

Where Re and Pr are Reynolds and Prandtl number, respectively. Einstein's equation was applied to compute the viscosity of SiO_2/water nanofluid [24].

$$\mu_{nf} = \frac{\mu_f}{(1-\phi)^{2.5}} \quad (33)$$

Furthermore, Maxwell's equation was used to calculate the thermal conductivity of SiO_2/water nanofluid [24].

$$k_{nf} = k_f \times \frac{k_s + 2k_f + 2\phi\left(k_s - k_f\right)}{k_s + 2k_f - \phi\left(k_s - k_f\right)} \quad (34)$$

Where k_f, k_s and k_{nf} are thermal conductivity of the base fluid, nanoparticle, and nanofluid, respectively. Specific heat capacity and density of nanofluid by equations (35) and (36) are calculated [24].

$$\rho_{eff} = (1-\phi)\rho_f + \phi\rho_s \quad (35)$$

4. Theoretical result and discussion

The governing equations by the computer program FORTRAN and 4th Runge Kutta method are solved. In Table 2, the thermal and radiation properties of the various components of photovoltaic-thermal systems used to solve the equations are presented.

The results of solving the governing equations for fluid (DI water) flow rate of 75 l/h and urban water consumption rate of 40 l/h are portrayed in Fig. 6. In this figure, Experimental results and simulation of the photovoltaic-thermal system were also compared. This chart shows the results acquired from the solution of the governing equations are close to the experimental data measured and enjoy an appropriate match.

In Fig. 7 experimental results with predicted temperatures for four components of the photovoltaic-thermal system such as photovoltaic panel, copper plate, the working fluid in the collector, and the urban water of storage tank for water working fluid have been compared.

In Fig. 8 simulation results and measured experimental data for 11-14 nm and concentration of 3wt% SiO_2/water nanofluid have been compared. As it is clear, the simulation results for this nanofluid, which have been compared with measured data, are acceptable.

In Fig. 9 measured results and predicted temperatures for four components of the PVT system such as PV panel,

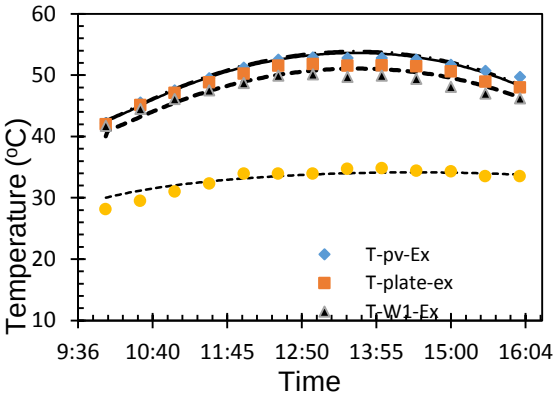

Figure 6. Comparison of the predicted and experimental temperature of different Component of photovoltaic thermal system for water as working fluid.

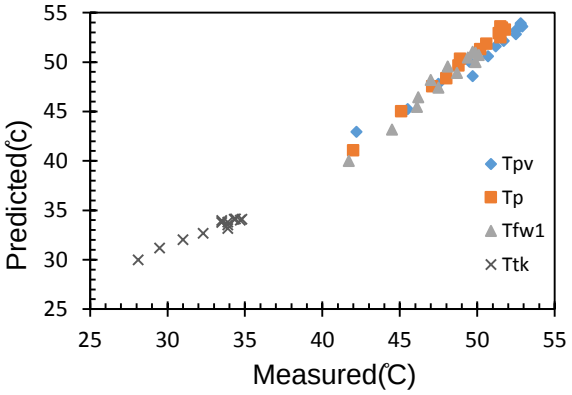

Figure 7. Measured and predicted Temperature of different component for water as working fluid.

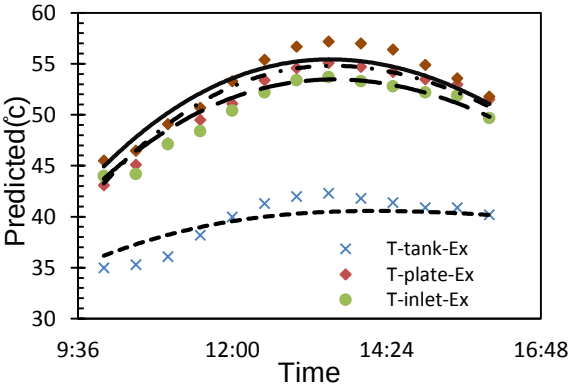

Figure 8. Comparison of predicted and experimental temperature of different component of photovoltaic thermal system for concentration of 3wt% and diameter of 11-14 nm SiO_2/water nanofluid as working fluid.

copper plate, the working fluid in the middle of collector and storage tank for 11-14 nm and concentration of 3wt% SiO_2/water nanofluid are decpited.

5. Analysis of DPVT system

The thermal performance of the flat-plate photovoltaic thermal system is like a conventional solar collector. In

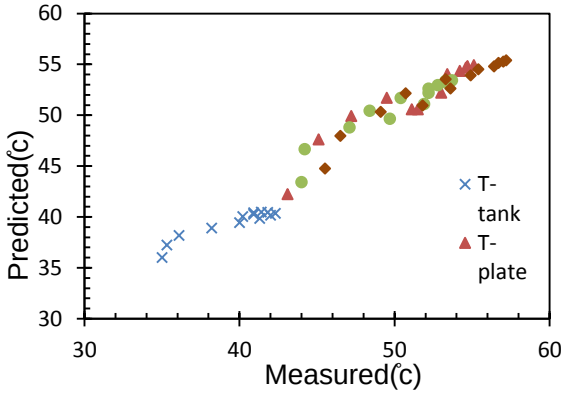

Figure 9. Measured and predicted Temperature of different component for concentration of 3wt% and diameter of 11-14 nm SiO_2/water nanofluid.

this system, the solar panel plays the role of a radiation absorbent. The thermal performance of the PVT system is obtained by Eq. (37) and (38).

$$\eta_{th} = \frac{Q_u}{GA} = \frac{\dot{m}C_p(T_o - T_i)}{GA} \quad (37)$$

where $\dot{m}$=75 l/h is the coolant mass flow rate, C_p is the specific heat capacity of working fluid, and T_o is the outlet temperature and T_i is the inlet temperature of the fluid. G is the incident solar radiation that is received by DPVT. In the present study surface area of DPVT collector (A) is 0.42 m^2.

$$\eta_{th} = F_R(\tau\alpha)_n + U_l\left(\frac{T_i - T_a}{G}\right) = a_1 + a_2\left(\frac{T_i - T_a}{G}\right) \quad (38)$$

$F_R(\tau\alpha)_n$ represents the rate of energy absorption by the collector, and F_RU_l is the coefficient of energy losses from the collector. In the above equation, η_{th} is the dependent variable, and T_i-T_a/G is the independent variable. In the plot of thermoelectrical performance $F_R(\tau\alpha)_n$ is where the graph meets the vertical axis. At this point, the ambient temperature and the inlet coolant temperature are equals, and the maximum value of collector efficiency occurs. The slope of the efficiency curve is equal to F_RU_l.

In addition, the electrical efficiency of DPVT system is acquired by the following Eq. (39):

$$\eta_{el} = \frac{VI}{GA} \quad (39)$$

Where V is the outlet voltage, and I is the outlet current. The overall efficiency of the photovoltaic system is obtained by summing thermoelectrical efficiency.

$$\eta_o = \eta_{th} + \eta_{el} \quad (40)$$

Moreover, primary-energy saving efficiency is calculated by Eq. (41). It indicates the value of the electricity produced is approximately three times the thermal energy.

$$\eta_{pr} = \eta_{th} + \frac{\eta_{el}}{0.38} \quad (41)$$

Where 0.38 is the efficiency of the electric power generation in a conventional power plant.

Table 2. Characteristics of different components for simulation.

Glass cover	Surface	A_g	m^2	0.537
	density	$_g\rho$	kg/m^3	2225
	emissivity	$_g\varepsilon$	-	0.88
	Extinction coefficient	λ	1/m	26
	Refractive index	N_v	-	1.5
	Specific heat capacity	$C_{p\,g}$	J/kg.k	835
	thickness	L_g	M	0.004
Photovoltaic panel	Cell surface	A_{pv}	m^2	0.429
	Packing factor	PF	-	0.84
	Temperature coefficient	$_c\varphi$	%	0.0045
	Reference cell efficiency	$_r\eta$	%	13.95
	Specific heat capacity	$C_{p\,pv}$	J/kg.k	903
	density	$_{pv}\rho$	kg/m^3	2702
Absorber plate	Thermal conductivity	k_p	W/m.k	310
	Specific heat capacity	$C_{p\,p}$	J/kg.k	385
	density	$_p\rho$	kg/m^3	8760
	thickness	L_p	mm	0.8
Cooper tube	Inner diameter	D_e	mm	7.5
	Outer diameter	D_o	mm	9.5
	Number of tubes	N	-	12
	Specific heat capacity	$C_{p\,t}$	J/kg.k	385
	density	$_t\rho$	kg/m^3	8760
	distance	-	m	0.05
Insolation layer	density	$_i\rho$	kg/m^3	10
	Refractive index	$C_{p\,i}$	J/kg.k	840
	Thermal conductivity	k_i	W/m.k	0.045
Storage tank	capacity	M_{tk}	L	40

6. Uncertainty analysis

In this research, an uncertainty analysis for thermoelectrical efficiency has been conducted. Data errors consist of measurements of flow rate, temperature, solar radiation, and current. In order to compute the uncertainty in the experiments, the Root Sum Square Method (RSSM) method is applied, which are presented in Eq. (42):

$$\left(S_{\eta th}\right)^2 = \left[\left(\frac{\Delta \dot{m}}{\dot{m}}\right)^2 + \left(\frac{\Delta((T_o - T_i))}{(T_o - T_i)}\right)^2 + \left(\frac{\Delta G}{G}\right)^2 + \left(\frac{\Delta A}{A}\right)^2\right] \quad (42)$$

The accuracy of the instruments used to measure quantities is reported in Table 3. These accuracies are applied for calculating the uncertainty of both thermo electrical efficiency.

The maximum computed uncertainty for thermal efficiency and electrical efficiency are ±0.0812 and ±0.0263, respectively. Both thermal and electrical efficiency uncertainty are under 10 percent that shows the experimental measurements are reliable.

7. Test procedures

In this experiment, the effect of the concentration of nanofluids, the average diameter of the nanoparticles, and the mass flow rate of urban water consumption on the thermoelectrical performance of photovoltaic-thermal

Table 3. accuracy of instruments

instrument	Measurement type	Unit	accuracy
K type thermocouples	Inlet and outlet Temperature	°C	0.1
Solar meter (TES 132)	Solar radiation	W/m^2	1
Digital multimeter (vector V97)	Voltage	Volt (V)	0.01
Digital multimeter (vector V97)	Current	Ampere (A)	0.001
Rotameter	Mass flow rate	kg/h	2

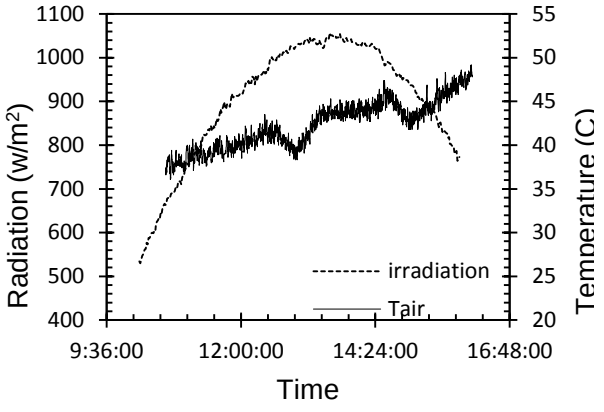

Figure 10. Daily variation of ambient temperature and irradiation.

Table 4. Summary of Experiments.

water/SiO_2 nanofluids	11-14 nm 1 wt%	11-14 nm 3 wt%	60-70 nm 1 wt%	60-70 nm 3 wt%
Urban water consumption	40-50-70 l/h			

Table 5. Installation condition of the DPVT system.

Location	Ahvaz, Khouzestan, Iran (Shahid Chamran University Of Ahvaz)
Latitude, Longitude	31.3°, 48.7°
Tilt angle	32°
Direction	south

systems are examined. Nanofluids employed in this study are at concentrations of 1wt% and 3wt%, and the average diameter of 11-14 nm and 60-70 nm, respectively. Further, volumetric flow rates of urban water consumption are 40, 50, and 70 liters per hour, respectively. The summary of the experiments is depicted in Table 4. The volumetric flow rate of the cooling fluid in a closed-loop cycle is 75 l/h.

The experiments were conducted during the hours 10 am to 4 pm. The process of testing has been in accordance with the ASHRAE standard. The pursuit of this standard flow rate, inlet and outlet temperature of working fluid (SiO_2/water nanofluid), ambient temperature, and radiation were measured. Fig. 10 portrayed the trends of the measured solar radiation and ambient air temperature. All the tests were performed in the same climatic conditions. The experimental conditions of the DPVT module are summarized in Table 5.

8. Experimental results and discussion

The thermal and electrical efficiency curves of the PVT system for different nanofluids and different urban water consumption rates in the figure of 11 to 18 are indicated. These curves include data points in which a linear regression has passed among them. In Fig. 11 thermal efficiency of DPVT system for nanofluid includes 1wt% concentration, and 11-14 nm SiO_2 nanoparticles in terms of mass flow rate are depicted. As it is evident, the thermal efficiency of DPVT in zero reduced temperature by increasing the mass flow rate from 40 to 70 kg/h, increases from 49.82% to 53.94. These numbers also for 60-70 nm SiO2 nanoparticles for alternating in mass flow rate from 40 and 70 kg/h are 47.98% and 52.83%, respectively (Fig. 13). These results exhibit an increase in mass flow rate causes Reynolds number increment, and eventually, thermal efficiency increases. As Figs. 11, 12, and 19 present, it can be observed that by increasing in nanofluid volume fraction from 1wt% to 3wt% for a mass flow rate of 40 kg/h and a nanoparticle size of 11-14, the thermal efficiency increased by 2.51%. This number for 50 and 70 kg/h is 1.81% and 2.27%, respectively. These alternations for 60-70 nm SiO2 nanoparticles for 40, 50 and 70 kg/h are 3.05%, 1.73% and 1.29%, respectively (Figs. 13 and 14). These values indicate that the effect of increasing the volume fraction is lower at a higher mass flow rate as a result of the lower average temperature and the decrease in the turbulence generated by nanoparticles in the fluid.

In the electrical part of this study, the amount of electrical efficiency with the change of volume fraction of nanoparticles, nanoparticle size, and rate of mass flow of urban consumed water was examined. As it was conducted in the thermal part as long as the rate of consumed water raised, heat removal from solar cell enhanced, and subsequently, electrical efficiency enhanced. In Fig. 15 electrical efficiency of DPVT system for nanofluid includes 1wt% concentration, and 11-14 nm SiO_2 nanoparticles in terms of mass flow rate are illustrated. The electrical efficiency of DPVT in zero reduced temperature by increasing the mass flow rate for 40, 50, and 70 kg/h are 8.27%, 8.43%, and 8.54%. These numbers for 60-70 nm SiO_2 nanoparticles are 8.14%, 8.32%, and 8.49%, respectively (Fig. 17). The results presented in Figs. 15 and 16 indicate that the increase in nanoparticle size causes electrical efficiency to deteriorate. By observing Figs. 15, 16, and 19, it can be seen that by increasing in nanofluid volume fraction from 1wt% to

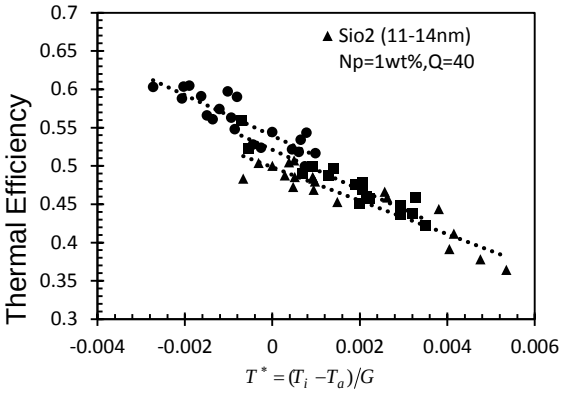

Figure 11. Thermal efficiency of the photovoltaic thermal system for 1wt% concentration and 11-14 nm of water/SiO_2 nanofluid.

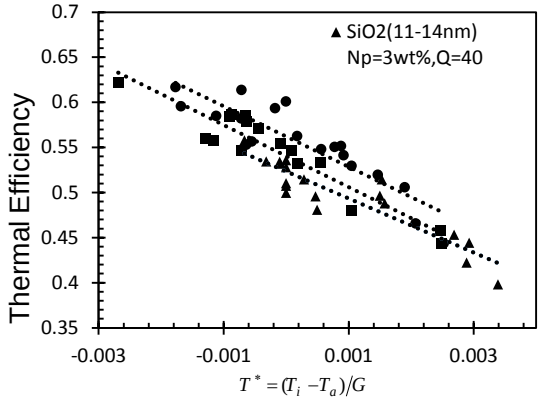

Figure 12. Thermal efficiency of the photovoltaic thermal system for 3wt% concentration and 11-14 nm of water/SiO_2 nanofluid.

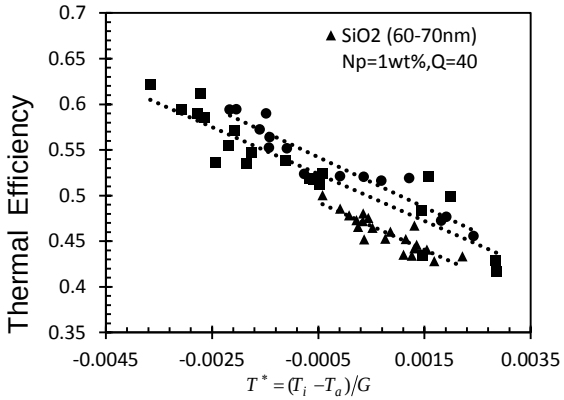

Figure 13. Thermal efficiency of the photovoltaic thermal system for 1wt% concentration and 60-70 nm of water/SiO_2 nanofluid.

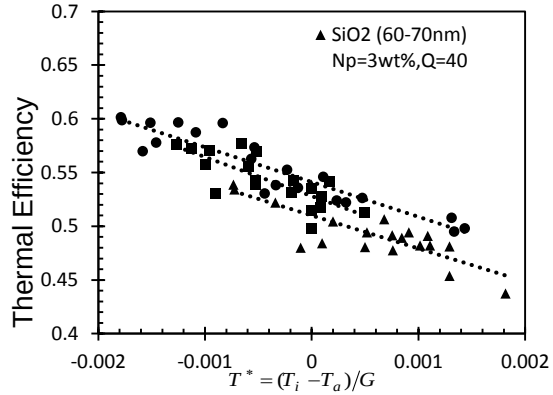

Figure 14. Thermal efficiency of the photovoltaic thermal system for 3wt% concentration and 60-70 nm of water/SiO_2 nanofluid.

3wt% for a mass flow rate of 40 kg/h and a nanoparticle size of 11-14, the electrical efficiency increased by 0.17%. This number for 50 and 70 kg/h are 0.9% and 0.21%, respectively. These alternates for 60-70 nm SiO_2 nanoparticles for 40, 50 and 70 kg/h are 0.25%, 0.16% and 0.14%, respectively (Figs. 17 and 18). the results confirm that the electrical efficiency enhances with the mass fraction of nanofluids, however, not significant.

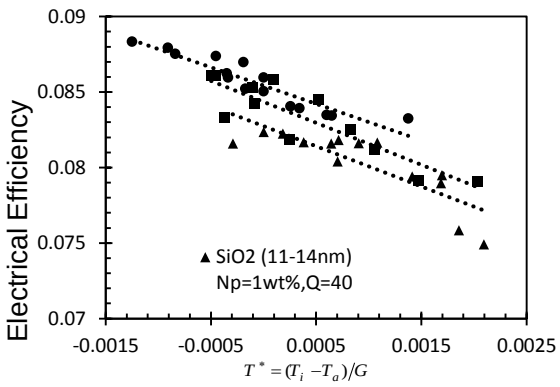

Figure 15. Electrical efficiency of the photovoltaic thermal system for 1wt% concentration and 11-14 nm of water/SiO_2 nanofluid.

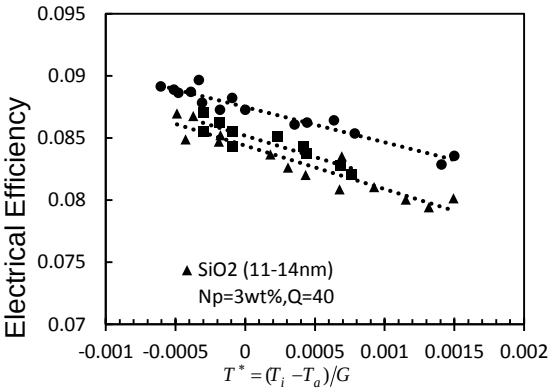

Figure 16. Electrical efficiency of the photovoltaic thermal system for 3wt% concentration and 11-14 nm of water/SiO_2 nanofluid.

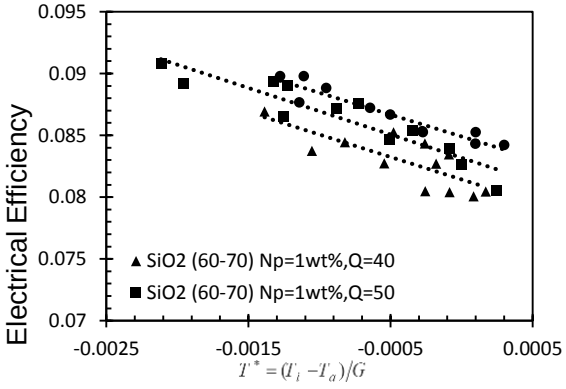

Figure 17. Electrical efficiency of the photovoltaic thermal system for 1wt% concentration and 60-70 nm of water/SiO_2 nanofluid.

As mentioned above, with a boost in the flow rate of the urban water, solar cell temperature drops; thus, the electrical efficiency increases. Furthermore, by an increase in the urban water flow rate, the average temperature of the storage tank is reduced; consequently, the temperature of the fluid entering the DPVT collector decreases. By reducing the inlet temperature to the collector, the average

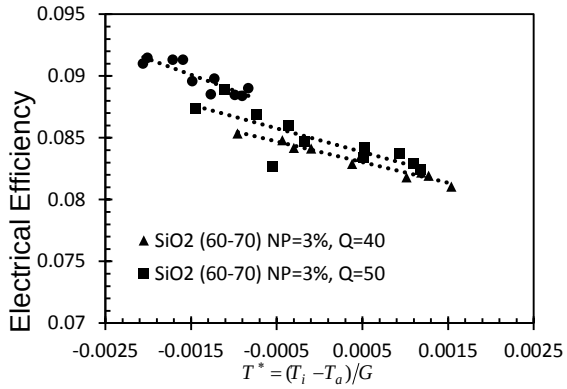

Figure 18. Electrical efficiency of the photovoltaic thermal system for 3wt% concentration and 60-70 nm of water/SiO_2 nanofluid.

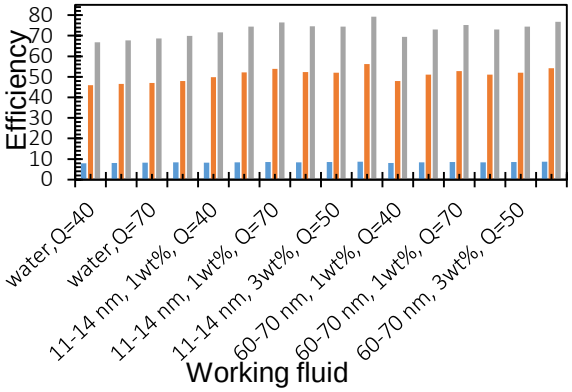

Figure 19. Thermal ( ), electrical ( ), and primary energy-saving efficiency ( ) of photovoltaic thermal system for the different working fluid.

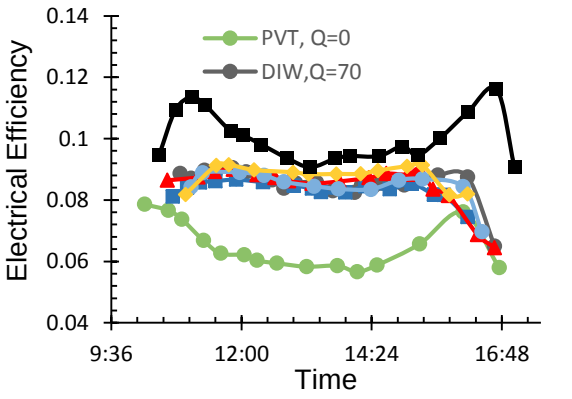

Figure 20. Daily variation of electrical efficiency of PVT system for different working fluid in the consumption rate of 70 L/h of urban water.

temperature of the DPVT system decreases and approaches the ambient temperature, and consequently, the heat losses decrease. Thus, it can be observed that for all nanofluids with an increase in the flow rate of urban water consumption, the thermal efficiency increases at zero reduced temperature. The average efficiency of DPVT system in zero reduced temperature is depicted in Table 6. Moreover, as protrayed in Fig. 19 for different nanofluids, with increasing urban water consumption rate

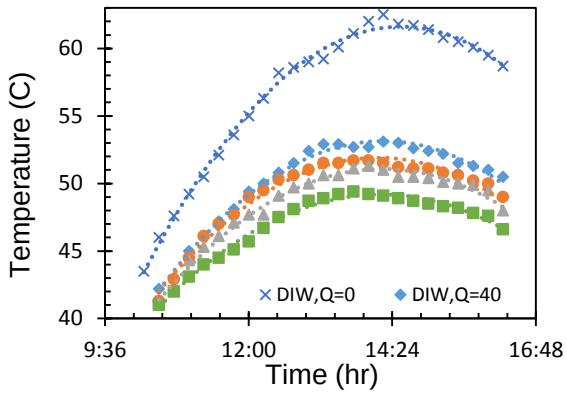

Figure 21. Daily variation of photovoltaic panel temperature with water as working fluid in the different consumption rate of urban water.

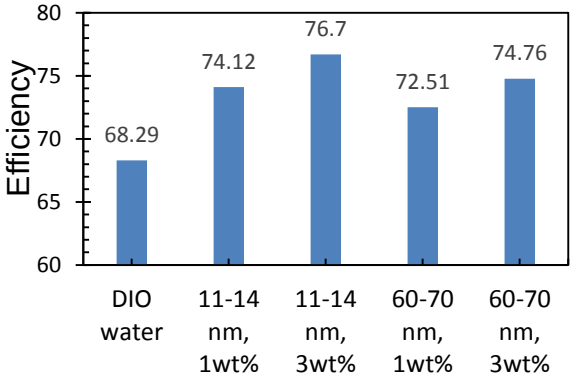

Figure 22. Average primary energy-saving efficiency of the photovoltaic thermal system for the different working fluid.

and reduction of the average temperature of the photovoltaic-thermal system, solar cell temperature decreases, and hence it increases electrical efficiency.

In Fig. 20 daily electrical efficiency of the PVT system for different working fluid is presented. Furthermore, in this figure, the daily variation of the electrical efficiency of the PVT system without withdrawing water from the storage tank (zero consumption rate) and photovoltaic panel (without thermal components) are indicated. Temperature variations of Photovoltaic panel for flow rates of urban water consumption for a typical experiment are depicted in Fig. 21.

The average overall efficiency of photovoltaic-thermal systems for all tests is presented in Fig. 22. This figure reveals through applying nanofluids as an alternative for the base fluid, the overall performance of the PVT system has been improved. The energy-saving efficiency of the system for 1wt% and 3wt% nanofluids with a diameter of 11-14 nm increased up to 5.83% and 8.41% than the base fluid, respectively. These values for nanofluids with 60-70 nm nanoparticle size are 4.22% and 6.47%. An increase in the overall efficiency of PVT systems is a result of the increase in the thermal conductivity of nanofluids than the water. With increasing volume fraction of nanofluids, the Brownian motion of nanoparticles increases, and with further disturbance of the fluid, the heat transfer

Table 6. Average efficiency of the PVT system at zero reduced temperature.

Working fluid	water	11-14 nm 1 wt%	11-14 nm 3 wt%	60-70 nm 1 wt%	60-70 nm 3 wt%
Thermal Efficiency	46.86	51.99	54.18	50.62	52.64
Electrical Efficiency	8.145	8.41	8.57	8.32	8.50
Overall Efficiency	55	60.4	62.76	58.94	61.14
Primary energy saving	68.29	74.12	76.74	72.51	75.01

coefficient increases. Fig. 20 indicates that the electrical performance of the photovoltaic- thermal system without exiting the water from the storage tank decreases greatly. The experimental results also illustrate that the performance of solar cells (without Thermal equipment) compared to all photovoltaic-thermal system experimen is higher. The reason for this phenomenon is that there is a glass cover on the solar cell in the photovoltaic-thermal system. This glass cover reduces the electrical efficiency due to the creation of the greenhouse effect, raising the temperature of the solar cell and the other hand, the reflection of sunlight. Existence of airflow around the solar cell in the photovoltaic system testing (without Thermal equipment) is another reason for increasing the electrical efficiency. Although the glass Cover reduces the electrical efficiency, because of the greenhouse effect, it significantly improves thermal efficiency. Therefore, adding thermal equipment to solar cells and producing thermal efficiency, thereby enhance the overall efficiency.

Domestic Photovoltaic-thermal (DPVT) collector with a closed-loop cooling system designed, built, and examined. Water/SiO_2 nanofluids were employed as a working fluid in a closed-loop cooling system. SiO_2 nanoparticles were applied due to the cheapness and excellent sustainability in water. In the experimental part, by alternating the concentration of nanofluids, the average diameter of the nanoparticles in nanofluids, and the urban water consumption rate, the thermo electrical performance of photovoltaic- thermal systems were examined. This work can be counted as a compact investigation on the thermal and electrical performance of the PVT system as there are not many reports in this field in literature, and all of them have reported some of the affecting parameters. In other words, the affecting parameters such as nanoparticles diameter, the mass concentration of nanoparticles in the base fluid, consumption rate of urban water have not been investigated simultaneously in literature. The results indicated that with the increase in urban water consumption, the overall system efficiency increased significantly. Therefore, the use of such a PVT system with nanofluid as a working fluid is suitable for domestic application. Affirmatively, one of the limitations of the use of nanoparticles is the deposition, and since the composition of water and SiO_2 is remarkably stable, this limitation has been removed to some extent.

Conclusion

In this study, a comprehensive theoretical and experimental work is conducted regarding the enhancement of the PV thermal performance using active cooling of water and SiO_2/water nanoflu. In the theoretical method, due to the CVFD method, an explicit dynamic prototype is developed. Performance of DPVT in thermal and electrical field are studied, and the effect of the mass fraction of nanofluids, the diameter of the nanoparticles are investigated. Nanofluid concentrations applied in this study were 1% and 3%, and the diameter of nanoparticles was 11-14 nm and 60-70 nm. The results of this study were as follows:

- The model which is employed for the PVT system using water and nanofluid (SiO_2/water) was in good agreement with test results, and the developed model can be applied for designs and efficiency evaluation of DPVT systems.
- Thermo electrical efficiency of DPVT systems has ameliorated in case SiO_2/Water nanofluids than water as a base fluid.
- The test results illustrated that with an increase in the urban water consumption rate, the average temperature of the system dropped and approached the ambient temperature. By reducing the temperature difference between the photovoltaic-thermal system and ambient temperature, the thermal efficiency meliorated. Consequently, with decreasing temperature, the electrical efficiency of photovoltaic cells increased.
- The results indicated that by increasing the urban water consumption rate for all working fluids, the overall performance increased. This increase includes improvement in thermoelectrical performance.
- Due to increasing nanofluids concentration of 1wt% to 3wt%, the electrical and thermal efficiency of the DPVT system amended. These values were 2.58% for nanoparticle with 11-14 nm of diameter and 2.25% for 60-70 nm. This phenomenon may be attributed to an increase in thermal conductivity as well as the increasing Brownian motion of particles in suspension.
- With enhancing of the average nanoparticles diameter, the overall performance of the photovoltaic-thermal system reduced. This reduction of nanofluids with a mass fraction of 1% and 3% is 1.61% and 1.94%, respectively. The reason for this phenomenon is most likely the decrease in the effect of Brownian motion for larger nanoparticles.

Nomenclature

H	Specific enthalpy [KJ/Kg]
I	Exergy destruction rate [KJ/Kg]
M	Mass flow rate [Kg/s]

P	Pressure [bar]
A	area
B	Angle of collector
C_P	specific heat
D	diameter
E	electrical output
f	colling fluid
FF	fill factor
F_R	heat removal factor
G	incident radiation
Gr	Grashohf number
h	Heat transfer coefficient
I	maximum power point current
k	thermal conductivity
L	length
$\dot{m}$	mass flow rate
Nu	Nusselt number
N_v	refractive index
PF	packing factor
r	reflection coefficient
T	temperature
T^*	reduced temperature
U_L	heat loss coefficient
V	maximum power point voltage
V_{wind}	wind speed

Greeks

α	absorptivity
β	angle of deviation
β_T	heat expansion coefficient
δ	uncertainty
ε	emissivity
ϕ	volume fraction
ϕ_l	latitude
ϕ_c	temperature coefficient
γ	angle with north
η	efficiency
λ	extinction coefficient
μ	viscosity
θ_l	angle between solar and glass
ρ	density
σ	stefan bolzmans constant
τ	transmissivity
ω	angle of solar time

Subscripts

a	ambient
ad	adhesive
bf	base fluid
c	collector
cd	conduction
cv	convection
el	electrical
W0	Inlet
W1	middle
W2	Outlet
g	Glass
ga	galvanized plate
i	insolation
nf	nanofluid
p	absorbent plate
pr	primary
pv	photovoltaic
t	Tube
th	thermal
tin	tin (metal)
tk	Tank
s	solid (nanoparticle)
r	radiation

Abbreviations

DPVT	Domestic photovoltaic thermal
TEM	transmission electron microscope
SEM	scanning electron microscope

Acknowledgements

The authors would like to thank Prof. E. Hajidavallo for his helpful comments during the development of this work.

References

[1] G. Barone, A. Buonomano, C. Forzano, A. Palombo, O. Panagopoulos, 2019, Experimentation, modelling and applications of a novel low-cost air-based photovoltaic thermal collector prototype, Energy Conversion and Management, 195, 1079-1097.

[2] H. Chen, Z. Li, Y. Xu, 2019, Evaluation and comparison of solar trigeneration systems based on photovoltaic thermal collectors for subtropical climates, Energy Conversion and Management, 199, 111959.

[3] P. Dupeyrat, C. Ménézo, M. Rommel, H.M. Henning, 2019, Efficient single glazed flat plate photovoltaic–thermal hybrid collector for domestic hot water system, Solar Energy, 85(7), 1457-1468.

[4] A. Tiwari, G. Tiwari, T.S. Bhatti, 2019, Performance evaluation of a semi-transparent photovoltaic thermal (SPVT) inverted absorber flat plate collector (IAFPC) for constant collection temperature (CCT) mode, Solar Energy, 186, 382-391.

[5] S. Bhattarai, J.H. Oh, S.H. Euh, G.K. Kafle, D.H. Kim, 2012, Simulation and model validation of sheet and tube type photovoltaic thermal solar system and conventional solar collecting system in transient states, Solar Energy Materials and Solar Cells, 103, 184-193.

[6] M.R. Saffarian, M. Moravej, M.H. Doranehgard, 2020, Heat transfer enhancement in a flat plate solar collector with different flow path shapes using nanofluid, Renewable Energy, 146, 2316-2329.

[7] A.R. Noghrehabadi, E. Hajidavalloo, M. Moravej, 2016, An experimental investigation of performance of a 3-D solar conical collector at different flow rates, Journal of Heat and Mass Transfer Research, 3(1), 57-66.
[8] D. Gürlich, A. Dalibard, U. Eicker, 2017, Photovoltaic-thermal hybrid collector performance for direct trigeneration in a European building retrofit case study, Energy and Buildings, 152, 701-717.
[9] H.A. Nasef, S. A. Nada, H. Hassan, 2019, Integrative passive and active cooling system using PCM and nanofluid for thermal regulation of concentrated photovoltaic solar cells, Energy Conversion and Management, 199, 112065.
[10] B. Bokor, H. Akhan, D. Eryener, L. Kajtár, 2017, Theoretical and experimental analysis on the passive cooling effect of transpired solar collectors, Energy and Buildings, 156, 109-120.
[11] T.T. Chow, W. He, J. Ji, 2007, An experimental study of facade-integrated photovoltaic/water-heating system, Applied thermal engineering, 27(1), 37-45.
[12] M. Rezvanpour, D. Borooghani, F. Torabi, M. Pazoki, 2020, Using CaCl2· 6H2O as a phase change material for thermo-regulation and enhancing photovoltaic panels' conversion efficiency: Experimental study and TRNSYS validation, Renewable Energy, 146, 1907-1921.
[13] W. He, Y. Zhang, J. Ji, 2011, Comparative experiment study on photovoltaic and thermal solar system under natural circulation of water, Applied Thermal Engineering, 31(16), 3369-3376.
[14] N. Abbas, M.B. Awan, M. Amer, S.M. Ammar, U. Sajjad, H.M. Ali & A.T. Jafry, 2019, Applications of nanofluids in photovoltaic thermal systems: a review of recent advances, Physica A: Statistical Mechanics and its Applications, 122513.
[15] A.R. Noghrehabadi, A. Esmaeilinasab, E. Hajidavalloo, 2014, The influence of urban water consumption on performance of domestic photovoltaic-thermal systems: an experimental investigation, International journal of energy & technology, 6 (22), 1–5.
[16] N. Karami, M. Rahimi, 2014, Heat transfer enhancement in a hybrid microchannel-photovoltaic cell using Boehmite nanofluid, International Communications in Heat and Mass Transfer, 55, 45-52.
[17] M. Sardarabadi, M. Passandideh-Fard, S.Z. Heris, 2014, Experimental investigation of the effects of silica/water nanofluid on PV/T (photovoltaic thermal units), Energy, 66, 264-272.
[18] Z. Xu, C. Kleinstreuer, 2014, Computational analysis of nanofluid cooling of high concentration photovoltaic cells, Journal of Thermal Science and Engineering Applications, 6(3), 031009.
[19] S. Bhattarai, J.H. Oh, S. H. Euh, G.K. Kafle, D.H. Kim, 2012, Simulation and model validation of sheet and tube type photovoltaic thermal solar system and conventional solar collecting system in transient states, Solar Energy Materials and Solar Cells, 103, 184-193.
[20] C. Stanciu, D. Stanciu, 2014, Optimum tilt angle for flat plate collectors all over the World–A declination dependence formula and comparisons of three solar radiation models, Energy Conversion and Management, 81, 133-143.
[21] F.P. Incropera, A.S. Lavine, T.L. Bergman, D.P. Dewitt, 2007, Fundamentals of heat and mass transfer, Wiley.
[22] R.S. Vajjha, D.K. Das, 2012, A review and analysis on influence of temperature and concentration of nanofluids on thermophysical properties, heat transfer and pumping power, International Journal of Heat and Mass Transfer, 55(15-16), 4063-4078.
[23] B.C. Pak, Y.I. Cho, 1998, Hydrodynamic and heat transfer study of dispersed fluids with submicron metallic oxide particles, Experimental Heat Transfer an International Journal, 11(2), 151-170.
[24] B. Ghasemi, S.M. Aminossadati, 2010, Brownian motion of nanoparticles in a triangular enclosure with natural convection, International Journal of Thermal Sciences, 49(6), 931-940.
[25] J.H. Watmuff, W.W. Charters, D. Proctor, 1977, Solar and wind induced external coefficients-solar collectors, Cooperation Mediterraneenne pour l'Energie Solaire, 56.